MAUSAM, **76**, 3 (July, 2025), 942-951

MAUSAM

DOI : https://doi.org/10.54302/mausam.v76i3.6932
Homepage: https://mausamjournal.imd.gov.in/index.php/MAUSAM

UDC No.551.554(512.317)

A further study of a special event of low-level windshear at the Hong Kong International Airport

P.W. CHAN[1*] and K.K. LAI[2]

[1]*Hong Kong Observatory, 134A Nathan Road, Kowloon, Hong Kong, China*

[2]*Hong Kong Observatory, Hong Kong, China* **(lai.kaikwong@gmail.com)**

(Received 26 December 2024, Accepted 09 May 2025)

***Corresponding author's email: pwchan@hko.gov.hk,**

सार – यह हांगकांग अंतर्राष्ट्रीय हवाई अड्डे पर एक विशेष पवन अवरूपण मामले का अनुवर्ती अध्ययन है। पिछले अध्ययन में, क्रॉस-माउंटेन वायु प्रवाह के लिए डॉपलर LIDAR द्वारा प्रेक्षित वायु प्रवाह विक्षोभ को अनुकरण में उचित रूप से पुन: प्रस्तुत किया जा सकता है, लेकिन दो पहलू हैं जो इतने संतोषजनक ढंग से अनुकरित नहीं किए गए हैं, पहला, तापमान और हवाई अड्डे के पश्चिम में समुद्र के ऊपर ऋतुनिष्ठ उत्प्लव पर ओसांक में झंप और दूसरा उस क्षेत्र में उत्क्रम वायु प्रवाह। यह अध्ययन इन दो विशेषताओं को पुन: प्रस्तुत करने के लिए कई मॉडल सेटअप पर विचार करता है, पहला, विभिन्न संख्यात्मक मौसम पूर्वानुमान मॉडल का उपयोग, ऊर्ध्वाधर समन्वय प्रणाली का विकल्प और दूसरा, प्रक्षोभ मापदंडीकरण योजना का विकल्प। यह पाया गया है कि MYNN प्रक्षोभ मापदंडीकरण योजना के साथ मौसम पूर्वानुमान और अनुसंधान (WRF) मॉडल का उपयोग सबसे अच्छे परिणाम देता है। ऊर्ध्वाधर समन्वय प्रणाली का विकल्प गौण प्रतीत होता है। तापमान और ओसांक में तेजी से गिरावट और वृद्धि के लिए तंत्र की आगे की जांच अनुकरण परिणाम के आधार पर की गई। वे हवाई अड्डे के क्षेत्र में प्रवाह व्यवस्था में अर्थात्, हवाई अड्डे से प्रचलित पूर्वी प्रवाह से, पहाड़ों को पार करने वाले अधिक दक्षिणी प्रवाह तक बदलाव से संबंधित पाए गए। यह अध्ययन मध्य मापक्रम संख्यात्मक मौसम पूर्वानुमान मॉडल का उपयोग करके उच्च स्थानिक संकल्प के साथ जटिल भूभाग के क्षेत्रों में पवन प्रवाह का अनुकरण करने के लिए एक संदर्भ के रूप में काम कर सकता है।

ABSTRACT. This is a follow-up study of a special windshear case at the Hong Kong International Airport. In the previous study, the airflow disturbances observed by the Doppler LIDAR for cross-mountain airflow could reasonably be reproduced in the simulation, but there are two aspects that are not simulated so satisfactorily, namely, the jumps in temperatures and dew points at the weather buoys over the sea to the west of the airport and the reverse airflow at that area. The present study considers a number of model setups in order to reproduce these two features, namely, the use of different numerical weather prediction models, the choice of vertical co-ordinate system and the choice of turbulence parameterization scheme. It is found that the use of Weather Forecasting and Research (WRF) model with MYNN turbulence parameterization scheme seems to give the best results. The choice of vertical co-ordinate system appears to be secondary. The mechanism for the rapid fall and rise in temperatures and dew points is investigated further based on the simulation result. They are found to be related to a change of the flow regime in the airport area, namely, from prevailing easterly flow from the airport, to a more southerly flow crossing the mountains. The present study may serve as a reference for simulating wind flow in areas of complex terrain with a high spatial resolution using mesoscale numerical weather prediction models.

Key words – Foehn wind, Windshear, High resolution modelling, Weather buoys.

1. Introduction

Low-level windshear refers to rapid and sustained changes of the headwind/tailwind to be encountered by an aircraft. It could be hazardous to aviation operation. At the Hong Kong International Airport (HKIA), the majority of low-level windshear is related to effect of complex terrain on the airflow. Forecasting of the occurrence of low-level windshear may help timely provision of relevant alerts to the air traffic controllers and pilots.

Numerical simulations using a mesoscale meteorological model have been conducted as an attempt to forecast the occurrence of low-level windshear. In particular, in Chan *et al*. (2021), the Regional Atmospheric Modelling System (RAMS) version 6.3 with Deardorff (1980) turbulence parameterization scheme is found to reproduce the airflow disturbances as revealed by the Doppler LIDARs at the HKIA. However, RAMS is using terrain following vertical co-ordinates. For the mountainous Lantau Island to the south of HKIA, the local slope may exceed 55 degrees, and the terrain following co-ordinates may not be sufficient to resolve the airflow along the relatively steep slopes.

Some recent developments of vertical co-ordinates for complex terrain, such as Weather Research and Forecasting Immersed Boundary Method (WRF-IBM, Arthur *et al*., 2018) would be adopted in the present study to find out any further improvements in the numerical simulation results in areas of complex terrain. The immersed boundary method (IBM), which uses a nonconforming grid and represents the topography by imposing boundary conditions along an immersed terrain surface, provides an alternative to terrain-following vertical coordinates. It is found to have a good representation of the airflow along the relatively steep slopes.

Apart from the choice of vertical co-ordinates, the choice of boundary layer scheme is also crucial in the simulation of small-scale (in the order of tens of metres) flow features in the HKIA area. There are only limited number of choices available for turbulence parameterization scheme in RAMS. In WRF, a number of more recently developed parameterization schemes are available, such as MYNN which is a local closure scheme of 1.5 orders which includes explicitly the effect of stability on the turbulent mixing length using Large Eddy Simulation (LES) model results. There are also more traditional schemes such as 1.5 - order local closure scheme MYJ and non-local, first-order scheme YSU. The MYNN scheme, similar to the MYJ, is a 1.5-order local closure scheme based on a prognostic equation for TKE. Unlike the MYJ scheme, which uses observations to derive expressions of stability and mixing length, the MYNN scheme uses results from LES to derive these expressions. A recent study of the various turbulence parameterization schemes could be found in Tito *et al*. (2024). In particular, the MYNN scheme is found to have the best performance for simulations with a spatial scale of several kilometres (*e.g*. Chen *et al*., 2024). The objective of the study is to find out its performance in an area of complex terrain, such as HKIA region, for simulations with a spatial resolution as fine as several tens of metres only.

The windshear case under consideration has been reported extensively in Chan (2023). Details of the case and the model setup would not be reproduced here. The model setup is similar to that reported in this previous study. In Chan (2023), the RAMS with Deardorff scheme is found to have reasonable reproduction of waves and vortices downstream of the mountains of Lantau Island, as well as the Foehn effect for cross-mountain airflow. However, the simulation results still show two important limitations - first, the fluctuations in temperatures and dew points as recorded at the weather buoys over the seas to the west of the airport could not be reproduced well; in particular, there are jumps of temperatures and dew points by a couple of degrees Celsius or more, which do not show up in the simulation results; second, the winds at the second runway (centre runway) of HKIA have too much southerly component; in reality the winds over and to the west of the airport seem to be convergence between the easterly flow and the southeasterly flow. The capability of the present model setups in simulating these features would be investigated in detail. The better representation of terrain in WRF-IBM model and the better expression of the stability in MYNN scheme may help improve the modelling deficiencies in temperature/dew point and southerly wind component. This is the motivation for the present study.

2. Data and methodology

One major limitation of the previous simulation in Chan (2023) is the choice of boundary condition. In that study, in order to simulate real-life application of the model, the forecast of NCEP (global forecasting system of National Oceanic and Atmospheric Administration of the US) is adopted as the boundary. However, there may be limitations of the real-time forecast models, so that downscaled simulation results may not be capable of reproducing the two major features about the surface temperature, dew point and wind as described above in the Introduction section. In the present study, the hourly re-analysis based on European Centre of Medium Range Weather Forecast (ECMWF) ERA-5 would be adopted as the boundary condition.

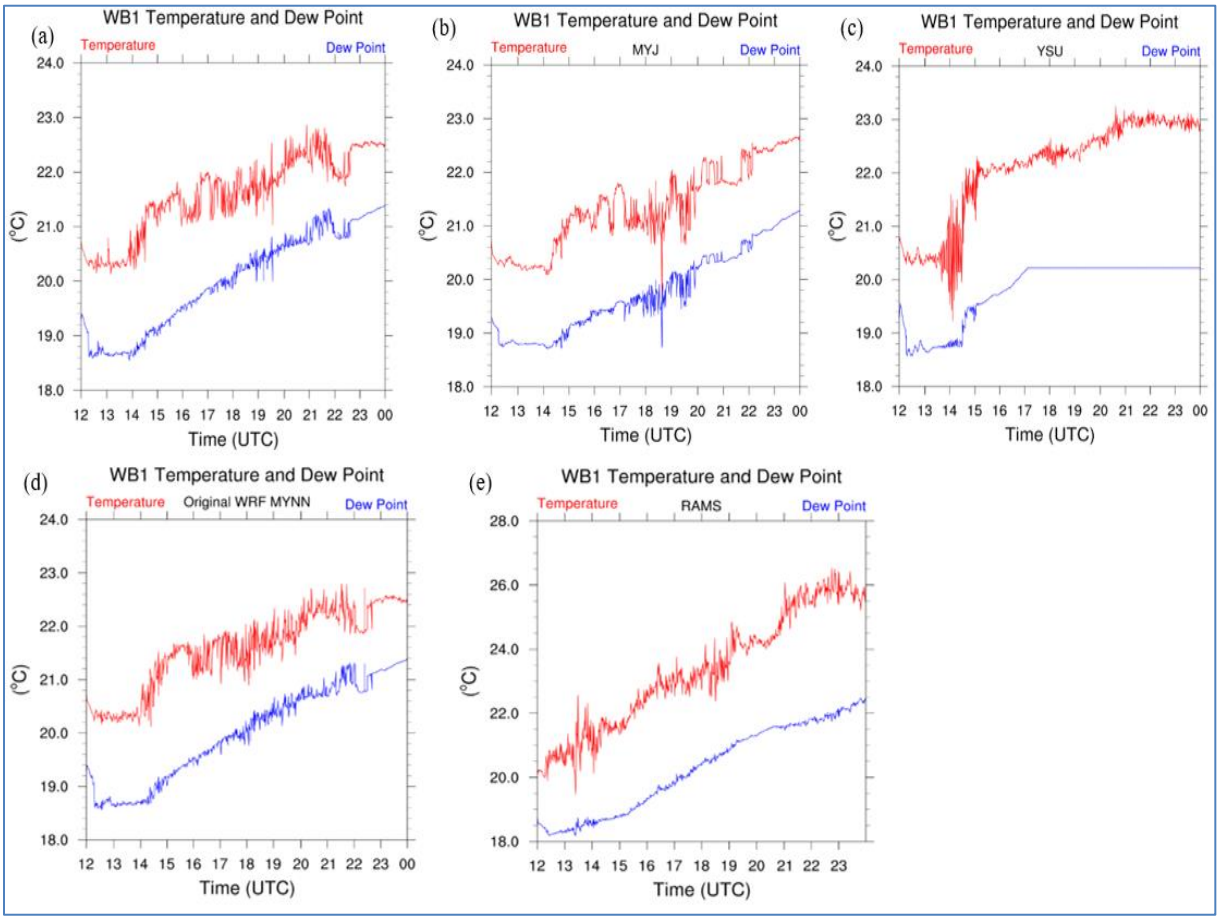

Figs. 1. (a) to (e) are the simulated time series of temperatures and dew points at location WB1 for model setup 1) to 5) respectively.

The present study aims at studying the followings: (*i*) the choice of different models, namely, RAMS vs WRF, with the use of RAMS as continuation with the previous study of Chan (2023), (*ii*) the choice of vertical co-ordinate system, namely, IBM vs terrain following, and (*iii*) the choice of boundary layer turbulence parameterization scheme. Based on these considerations, the following five model setups has been adopted:

(*i*) MYNN based on WRF-IBM

(*ii*) MYJ based on WRF-IBM;

(*iii*) YSU based on WRF-IBM;

(*iv*) MYNN based on terrain following co-ordinate system of the "ordinary" WRF with the same version of WRF-IBM (version 3.6); and

(*v*) RAMS with Deardorff, as the baseline.

Only dynamic downscaling is performed. There is no assimilation of actual data. The innermost grid, which is the grid with the results presented in the following sections), has a horizontal resolution of 40 m. The models are initialized at 12 UTC, 24 March 2022, and run for 12 hours.

3. Results and discussion

3.1. *Weather buoy simulation results*

As studied in Chan (2023), the three weather buoys to the west of HKIA would be considered, namely, WB1, WB2 and WB5. The major consideration would be put on the simulation of temperatures and dew points at the buoys.

For WB1, the results from the five model runs are shown in Fig. 1. Compared to the results of RAMS in Chan (2023), the present model setups generally reproduce larger fluctuations of the temperatures and dew points as observed in actual measurements, especially for

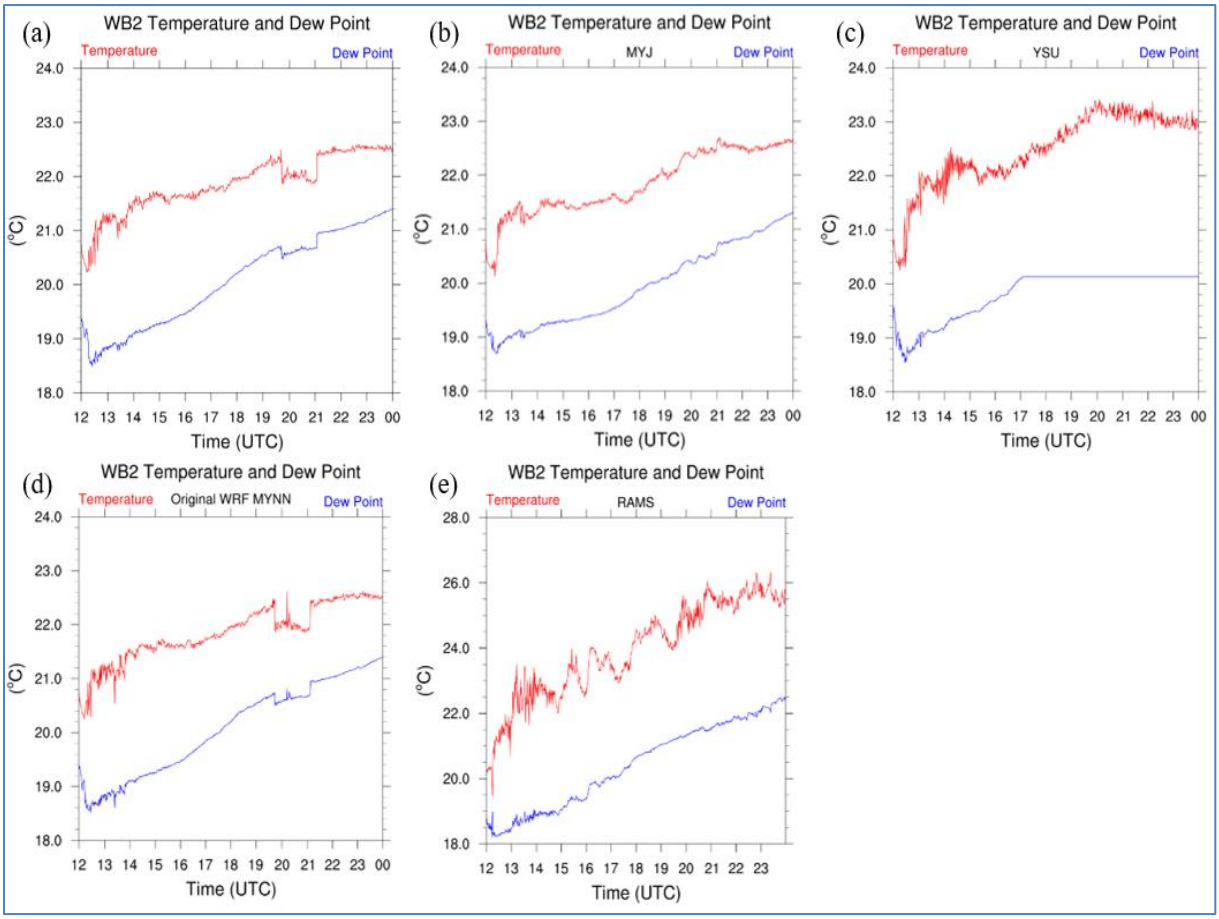

Figs. 2 (a) to (e) are the simulated time series of temperatures and dew points at location WB2 for model setup 1) to 5) respectively

setups (*i*), *(ii*), (*iv*) and (*v*), with the adoption of ECMWF hourly re-analysis playing a major role. However, setup (*iii*) is still smoother in the simulated temperature trace, and there is a "plateau" of dew point at the time of around 17 UTC onwards. The simulation inputs and outputs have been double-checked, and this "plateau" should not be artificial.

However, compared to the actual observations in Chan (2023), the "spikes" of the simulated temperatures are still rather low and the maximum change of temperature is in the order of one degree Celsius only. The underestimation may be related to the rather limited spatial resolution of the model (40 m only) as well as the presentation of the turbulence in the model (only 1.5 order turbulence parameterization scheme is adopted in the modelling).

The simulated results for WB2 are shown in Fig. 2. With the use of MYNN, for whichever vertical co-ordinate system (setups (*ii*) and (*iv*)), sharp falls and rises of temperatures and dew points have been successfully reproduced, which are observed in actual measurements (Chan (2023)). The temperature and dew point traces are smoother in setups (*ii*) and (*iii*). Rises and falls are also captured in setup (*v*) but not as sharp as setups (*i*) and (*iv*). As such, it is found that choice of turbulence parameterization scheme within the same model (WRF) iscrucial in reproducing the temperature and dew point fluctuations. In general WRF-MYNN performs better than RAMS-Deardorff. The choice of vertical co-ordinate system (setup 1) vs setup 4)) does not seem to play a major role. The temperature/dew point changes are mostly related to the larger scale features of the mountainous Lantau terrain instead of the individual, local slopes, and as such the benefits of WRF-IBM model may not be reflected in the simulation results in comparison with the actual observations.

Similar conclusions maybe drawn for the simulations for WB5 (Fig. 3). For this case, not just the sharp fall and rise of temperature/dew point could be reproduced by the choice of MYNN turbulence parameterization scheme

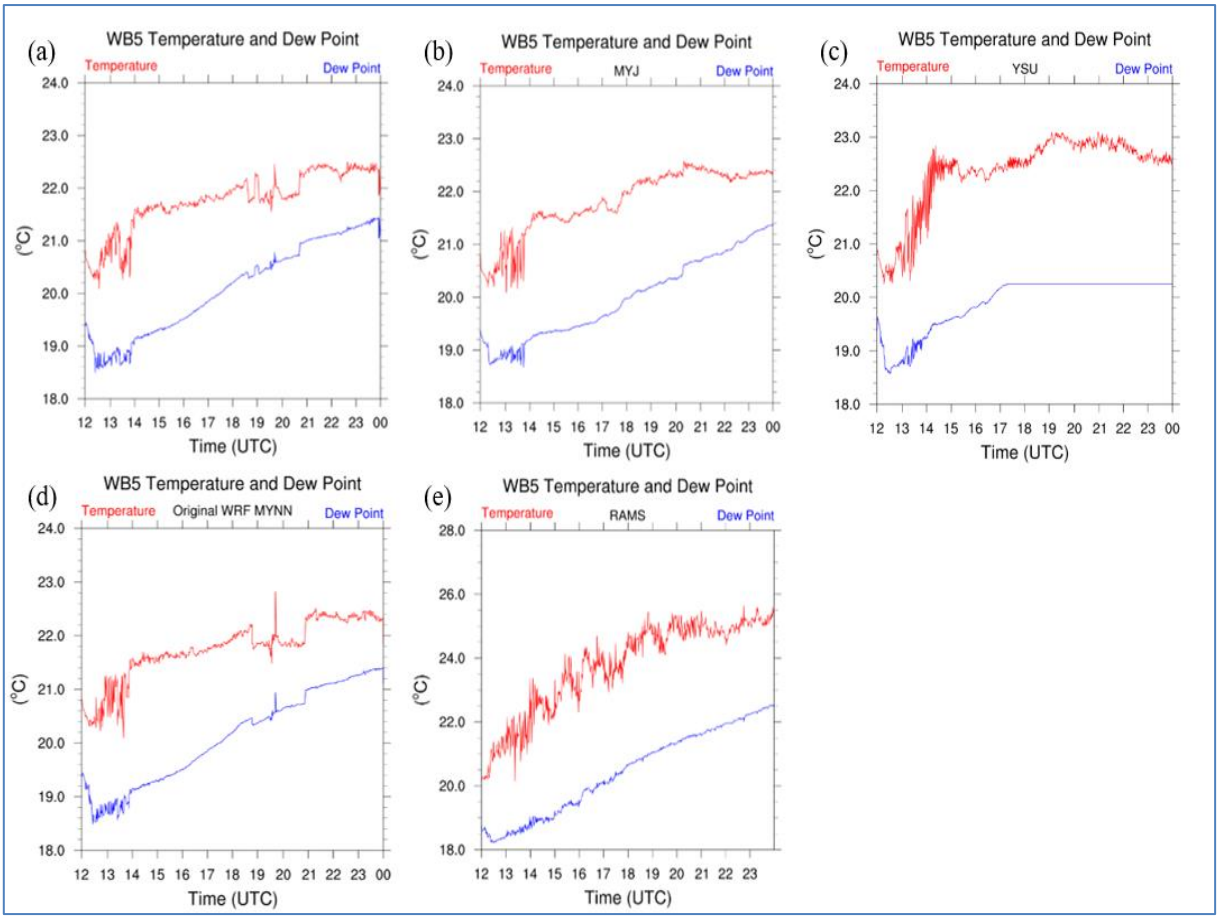

Figs. 3. (a) to (e) are the simulated time series of temperatures and dew points at location WB5 for model setup 1) to 5) respectively.

(setups (*i*)) and (*iv*)), there is also a very sharp spike of temperature simulated in setup 4). This spike is observed in reality for WB1 (Chan, 2024), but this minor difference in the locations of the two buoys (WB1 vs WB5) is considered to be acceptable for such fine-scale simulation downscaled dynamically from a global model with a coarse spatial resolution. Choice of vertical co-ordinate seems to matter, namely, setup (*iv*) seems to better than setup (*i*) in terms of the magnitude of the spike.

Based on the above results, the use of WRF-IBM or the ordinary WRF with the choice of MYNN turbulence parameterization is considered to give the best simulations, considering the temperatures and dew points as measured at the buoys.

3.2. *Wind pattern simulation results*

The simulated surface wind patterns (10 metres above local ground level) for the five setups are shown in Fig.s 4(a) to 4(e). At the time instance with the simulated occurrence of reverse flow at the location of WB1 (surface wind with northerly component vs the prevailing southerly flow) is considered. At the same time, the wind pattern over the airport island would be studied at the same time. In all the five model setups, cross-mountain flow is simulated over southern part of airport island and the seas to the west of HKIA, with the occurrence of Foehn effect (higher surface temperatures). For the WRF runs (model setups (*i*) and (*iv*)), the models manage to reproduce the generally easterly flow over the north and the centre runway of HKIA, and the southeasterly flow to the west of the sea. On the other hand, similar to the previous study (Chan, 2023), RAMS (model setup (*v*)) has got too much southerly component for the surface winds over the airport island, up to the north runway and beyond.

Moreover, for northerly component wind (reverse flow) at the location of WB1, the MYNN of WRF appears to have better performance, no matter whether it is IBM or terrain-following vertical co-ordinate system.

Considering both the temperatures and dew points at weather buoys as well as the surface wind pattern, WRF

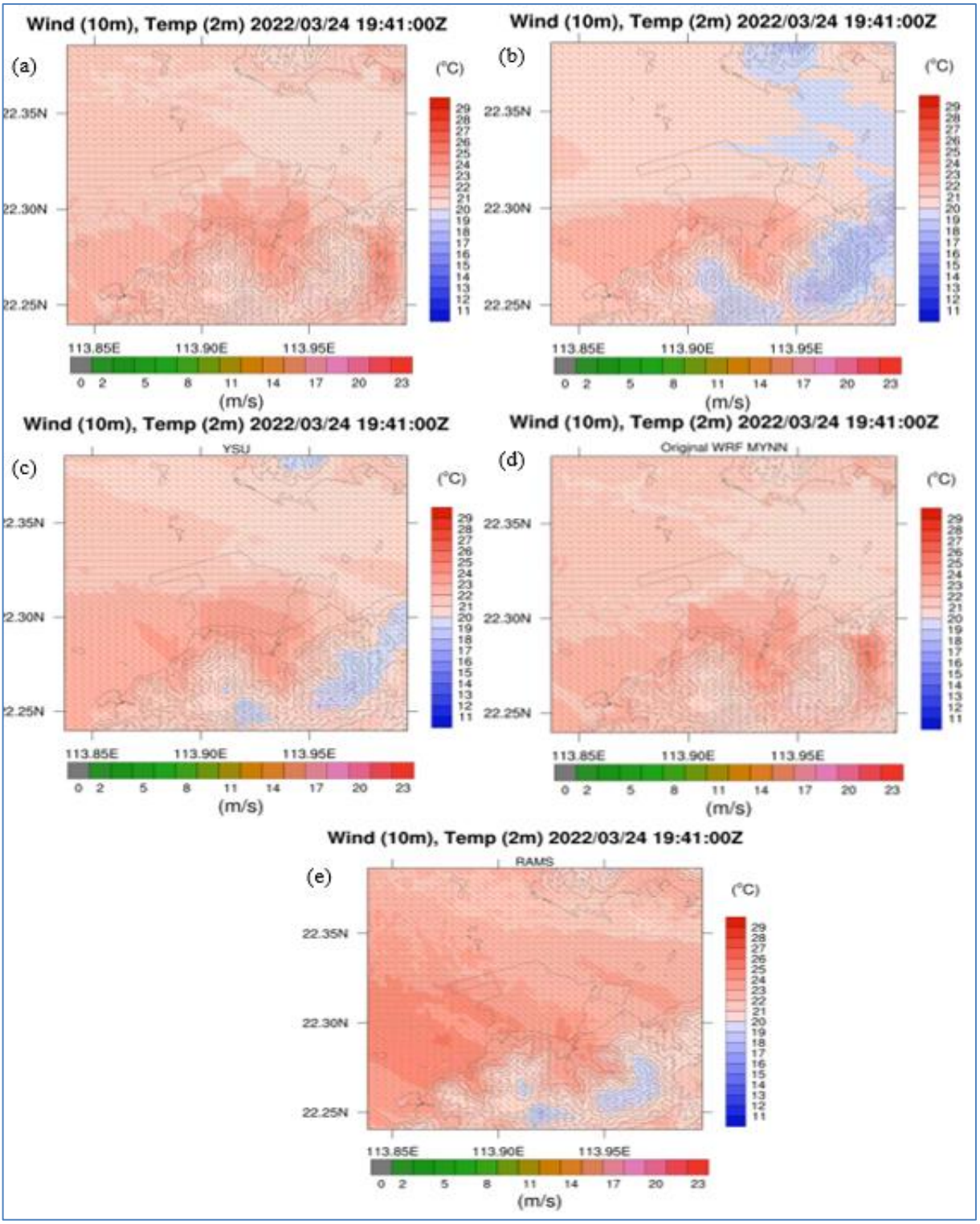

Fig. 4. The simulated surface wind (wind barb) and surface temperature (coloured shaded) for model setups 1) to 5) are shown in (a) to (e) respectively at the time 19:41:00 UTC.

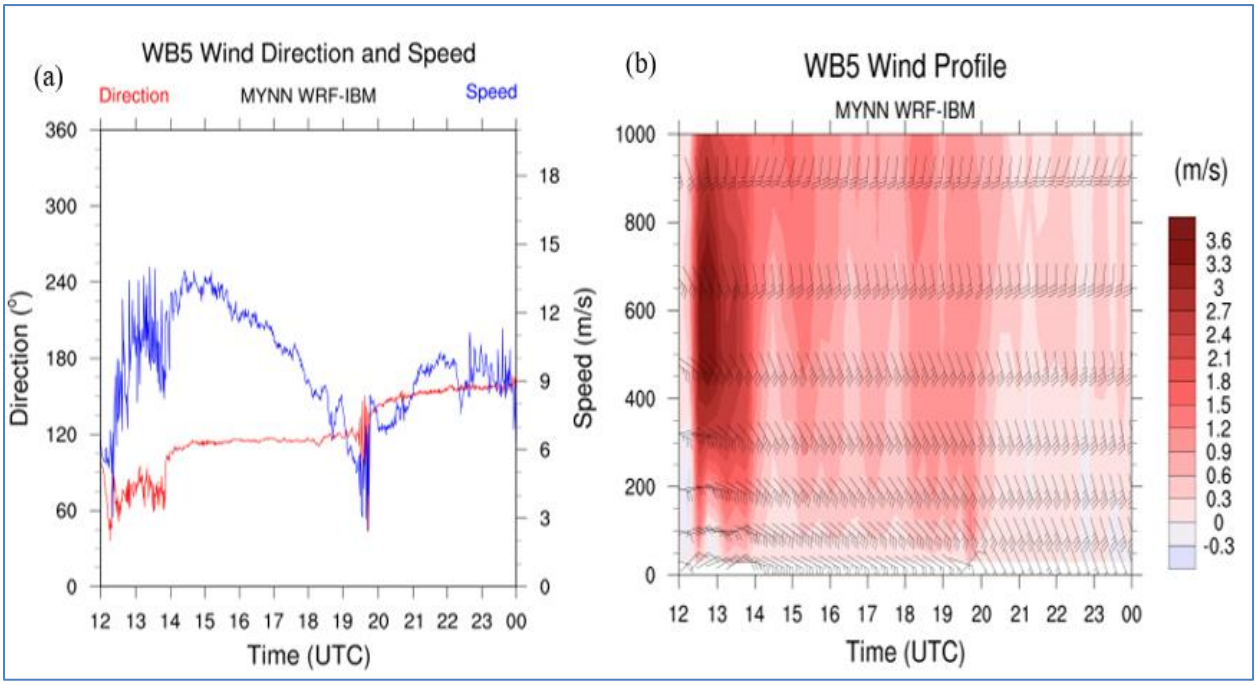

Figs. 5. (a) is the simulated time series of wind speed and wind direction at WB5, and (b) is the simulated vertical velocity (colour shaded) and wind (wind barb) at the atmospheric boundary layer at location WB5.

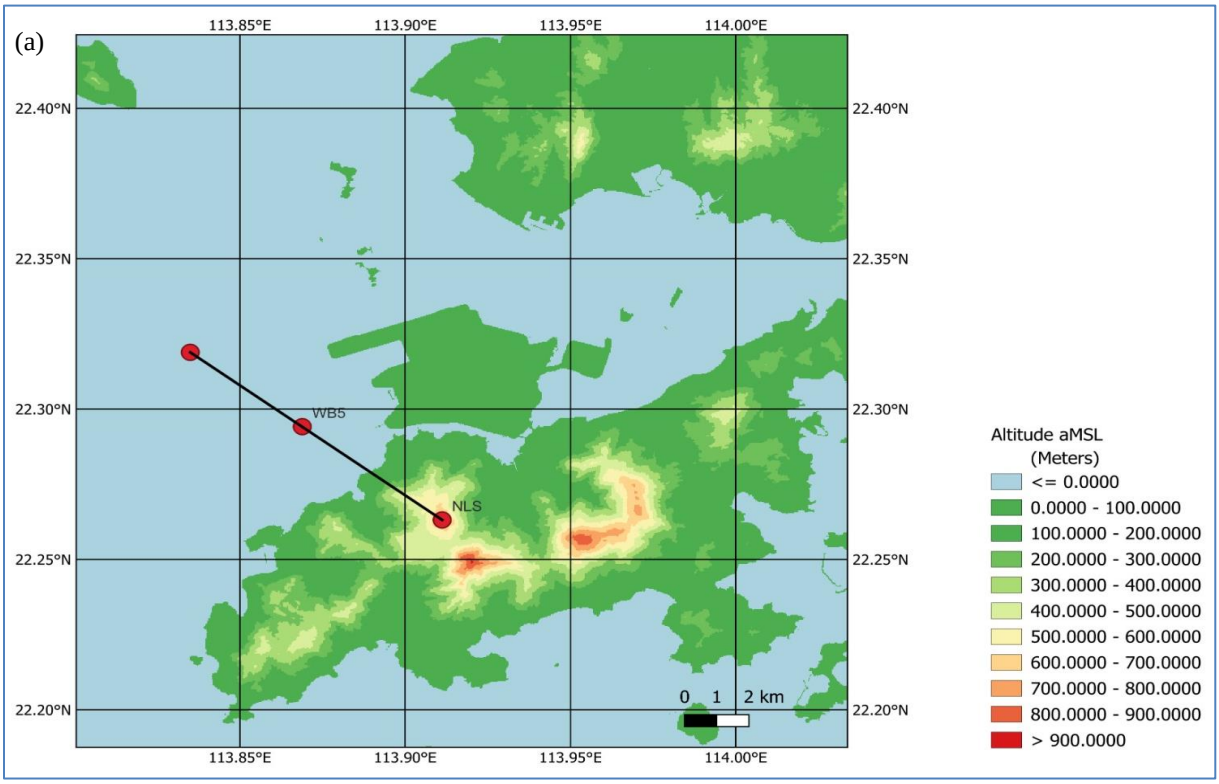

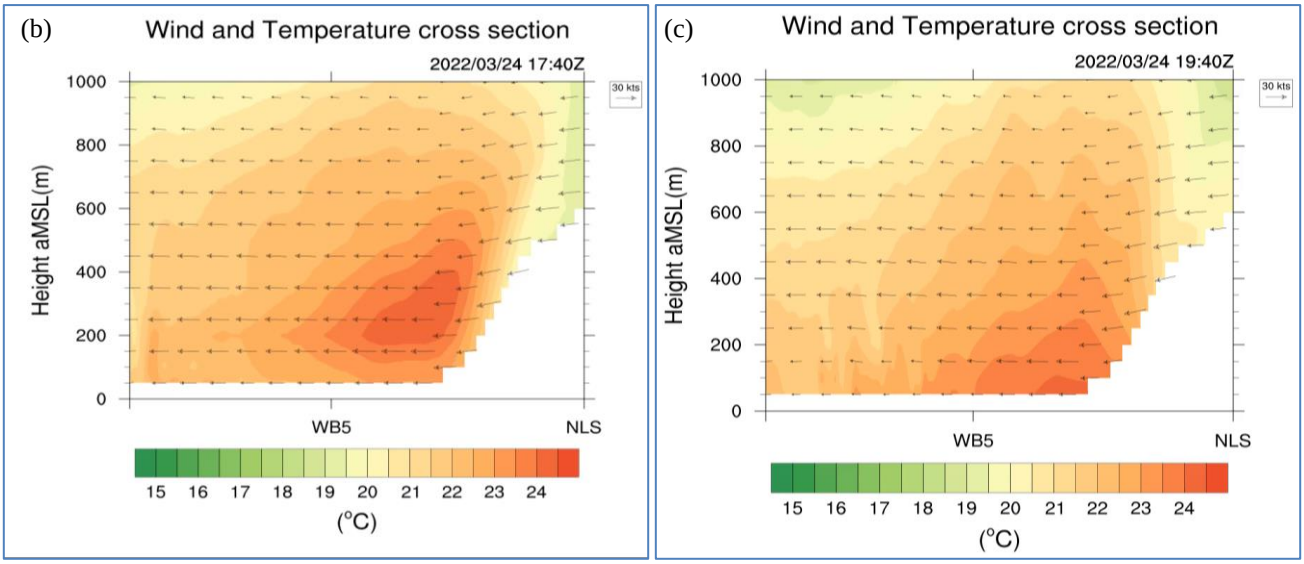

Fig. 6. (a), (b) & (c). Location of vertical cross section is shown in (a). (b) and (c) are the wind vector projected on the cross sectional plane (arrow) and temperature (colour shaded) at the vertical cross section for two time instances as shown in the figures.

TABLE 1

Error statistics based on data of WB1 – the three numbers are root-mean-square-error (left), best-fit equation (upper right, y is the model result and x is the observation) and correlation coefficient (lower right).

WB1	Wind Direction		Wind Speed		Temp(ºC)		Dew Point(ºC)	
MYJ	48.83491	y = 0.2957x + 71.181 R^2 = 0.5869	3.264518	y = -1.6035x + 23.869 R^2 = 0.3877	5.176466	y = 0.3491x + 12.155 R^2 = 0.7754	4.760543	y = 0.4257x + 9.3722 R^2 = 0.6586
MYNN	44.83727	y = 0.3482x + 70.649 R^2 = 0.6363	3.504939	y = -1.4166x + 20.95 R^2 = 0.3541	4.963145	y = 0.3549x + 12.215 R^2 = 0.8726	4.499812	y = 0.5516x + 6.524 R^2 = 0.8233
YSU	37.81688	y = 0.4212x + 68.871 R^2 = 0.8663	2.322643	y = -0.9378x + 18.706 R^2 = 0.3326	4.440254	y = 0.4746x + 9.5414 R^2 = 0.9218	4.724589	y = 0.3787x + 10.551 R^2 = 0.9449
RAMS	46.5648	y = 0.3379x + 67.019 R^2 = 0.6186	2.783457	y = -1.0026x + 19.529 R^2 = 0.2109	3.214141	y = 0.8471x + 0.9617 R^2 = 0.7464	4.220604	y = 0.842x - 0.3082 R^2 = 0.8019

TABLE 2

Error statistics based on data of WB2 – the three numbers are root-mean-square-error (left), best-fit equation (upper right, y is the model result and x is the observation) and correlation coefficient (lower right).

WB2	Wind Direction		Wind Speed		Temp(ºC)		Dew Point(ºC)	
MYJ	42.52434	y = 0.9971x - 41.67 R^2 = 0.8835	4.02356	y = 0.49x + 7.5037 R^2 = 0.0522	3.663061	y = 0.1036x + 19.217 R^2 = 0.0144	4.011748	y = 0.7678x + 1.5675 R^2 = 0.7505
MYNN	40.87718	y = 1.1439x - 64.257 R^2 = 0.819	3.857784	y = 0.0252x + 11.184 R^2 = 0.0001	3.651395	y = 0.0102x + 21.607 R^2 = 0.0002	3.871057	y = 0.9423x - 2.479 R^2 = 0.8736
YSU	37.36379	y = 1.1442x - 61.095 R^2 = 0.8822	3.581031	y = 0.5251x + 7.0994 R^2 = 0.094	3.105947	y = -0.1047x + 25.135 R^2 = 0.011	4.145416	y = 0.5188x + 7.3918 R^2 = 0.9387
RAMS	50.02022	y = 1.5152x - 135.74 R^2 = 0.8957	2.849019	y = 1.1194x + 0.7194 R^2 = 0.2946	2.135072	y = 0.088x + 21.701 R^2 = 0.0016	3.574772	y = 1.4543x - 14.399 R^2 = 0.8764

TABLE 3

Error statistics based on data of WB5 – the three numbers are root-mean-square-error (left), best-fit equation (upper right, y is the model result and x is the observation) and correlation coefficient (lower right).

WB5	Wind Direction		Wind Speed		Temp(ºC)		Dew Point(ºC)	
MYJ	35.92224	y = 0.8078x - 4.1036	3.305181	y = 0.1312x + 9.5684	3.091774	y = 0.6137x + 6.5427	2.987679	y = 1.0831x - 4.8769
		R^2 = 0.7951		R^2 = 0.0181		R^2 = 0.9327		R^2 = 0.8026
MYNN	34.59628	y = 0.8991x - 16.845	3.148646	y = -0.0438x + 10.179	3.141264	y = 0.5394x + 8.3511	2.878166	y = 1.2743x - 9.1553
		R^2 = 0.8081		R^2 = 0.0019		R^2 = 0.9018		R^2 = 0.8742
YSU	29.26103	y = 0.8544x - 3.6801	2.875204	y = 0.2244x + 8.6908	2.564619	y = 0.6483x + 6.2236	3.072475	y = 0.6977x + 3.8827
		R^2 = 0.7708		R^2 = 0.0903		R^2 = 0.7922		R^2 = 0.7916
RAMS	41.97046	y = 1.0892x - 54.639	3.52155	y = 0.5867x + 6.2842	1.261988	y = 1.4347x - 11.939	2.638569	y = 2.001x - 25.503
		R^2 = 0.9068		R^2 = 0.2389		R^2 = 0.9163		R^2 = 0.8841

MYNN (model setup (*i*) and (*iv*)) seems to have the best performance and manage to capture the minor features of the Foehn wind and the airflow in the HKIA area for this single case.

Further study of the temperature changes with the use of MYNN parameterization scheme.

The section attempts to briefly address why there are jumps (a fall followed by a rise) in temperature and dew point at WB5 in the simulation results for WRF MYNN, in order to understand the dynamics and thermodynamics of the jumps in the actual observations. First of all, the surface wind speed and wind direction at the location of WB5 are shown in Fig. 5(a). In the period between the two jumps, the wind speed has reached the lowest values and the wind direction is changing gradually from around 120 degrees relative to north, to around 150 degrees. At the same time, the upper air winds do not change much (Fig. 5(b)) and there is slight upward motion of the air in the atmospheric boundary layer (Fig. 5(b)). Therefore, in the period in between the jumps, there should be change of the flow regime at the location of the buoys, gaining more southerly component with weaker winds. In fact, around that time (Fig. 4), the buoys are located in the convergence zone between the easterly and southeasterly flow. Later on (not shown) the southeasterly flow will dominate over the seas to the west of the airport.

To study the change of the flow regime in more detail, a vertical cross section from a mountain top to the WB5 location is made in the simulation, with the location of the cross section shown in Fig. 6(a). Earlier on, as shown in Fig. 6(b), the cross mountain southeasterly flow leads to subsidence warming downhill, but the warming area does not reach the surface. At the location of WB5, the flow is still the relatively cooler easterly wind from the airport island. Some time later (Fig. 6(c)), the subsidence warming area extends to the sea surface, including the location of WB5. This is also the time when southeasterly flow prevails over the sea to the west of the airport (not shown). At the convergence line between easterly and southeasterly wind, there are small areas of warming (indicated by arrows in Fig. 6(c)), passing across WB5 from time to time. They give rise to the temperature fluctuations at that location.

3.3. *Error statistics*

To have a quantitative appreciation of the performance of the various model runs, the modelling results of WRF-IBM run for MYJ, MYNN and YSU as well as the original RAMS run are compared with the actual observations from the weather buoys WB1, WB2 and WB5 in the simulation period, and the they are presented in Tables 1 to 3 respectively. The elements under consideration include wind direction, wind speed, temperature and dew point. Three quantities are considered, namely, root-mean-square-error (RMSE), equation of the best-fit straight line (y as the model result and x as the actual observation) and the correlation coefficient (R^2) of the best-fit straight line.

In terms of the numbers, WRF-IBM run with YSU parameterization scheme in general has the best performance among the three WRF runs and the WRF-YSU results and RAMS results are comparable in terms of the error statistics. However, it is noted that the error statistics reflect the general performance of the models only, but not the capturing of the special features as

discussed earlier in the model, namely, the abrupt drop and rise as well as the spikes in the temperature and dew point, as well as the general pattern of the wind speed and direction. As such, WRF-IBM run with YSU and RAMS run are able to capture the general features of the flow rather well, but the noticeable features that are of operational interest may not be properly reflected in the modelling results. In fact, the error statistics of WRF-IBM run with MYNN are not particularly poor and may be considered to be comparable with those of WRF-IBM run with YSU for most of the cases.

4. Conclusions

This paper describes a number of model setups for simulating two specific aspects of the flow in a windshear case at HKIA, namely, the temperature and dew point fluctuations as observed at the weather buoys to the west of the airport, and the reverse flow as recorded by the buoys, both of which are not successfully simulated in the previous study of Chan (2023). Different models have been used (RAMS vs WRF). For WRF, there are different trials of vertical co-ordinates (terrain following vs IBM). For WRF-IBM, different turbulence parameterization schemes have been tried out (MYNN, MYJ and YSU). Among the different setups, the WRF-MYNN appears to have the best performance, at least in reproducing the features of interest.

The temperature and dew point fluctuations at the buoys are studied further. Their rapid fall and rise are found to be related to a change of the flow regime, namely, between the prevailing surface easterly and the cross-mountain southeasterly. This is evident from both the surface observations and the vertical cross-section of the airflow.

The present conclusions are based on one particular case of windshear at HKIA only. More cases and experiments would be conducted to find the most suitable model setup for simulating/forecasting the flow and temperature/dew point features as recorded at HKIA. Nonetheless, the results obtained in the present study are expected to be useful reference for operational forecasting of airflow in other airports with complex terrain.

Authors' Contributions

P.W. Chan: Conceptualization, writing and investigation.
K.K. Lai: Software and data curation.

Disclaimer: The contents and views expressed in this study are the views of the authors and do not necessarily reflect the views of the organizations they belong to.

References

Arthur, R. S., Lundquist, K. A., Mirocha, J. D., Chow, F. K., Topographic Effects on Radiation in the WRF Model with the Immersed Boundary Method: Implementation, Validation, and Application to Complex Terrain, *Mon. Weather. Rev*. 2018, 146, 3277-3292. doi : https://doi.org/10.1175/MWR-D-18-0108.1.

Chan, P. W., 2023, "Case study of a special event of low-level windshear and turbulence at the Hong Kong International Airport" *Atmospheric Science Letters*, **24**, e1143. doi : https://doi.org/ 10.1002/asl.1143.

Chan, P. W., K. K. Lai, and Q. S. Li, 2021, "High-resolution (40 m) simulation of a severe case of low-level windshear at the Hong Kong International Airport-Comparison with observations and skills in windshear alerting", *Meteorological Applications*, **28**, e2020

Chen, D. and coauthors, 2024, "Sensitivity analysis of planetary boundary layer parameterization on meteorological simulations in the Yangtze river delta region", *China. Environ. Sci*., Atmos., **4**, 1129-1144, doi : 10.1039/D4EA00038B.

Tito, Janet Valdés, Amauri Pereira de Oliveira, Maciel Piñero Sánchez, and Adalgiza Fornaro. 2024, "Evaluation of Nine Planetary Boundary Layer Turbulence Parameterization Schemes of the Weather Research and Forecasting Model Applied to Simulate Planetary Boundary Layer Surface Properties in the Metropolitan Region of São Paulo Megacity, Brazil" *Atmosphere* 15, no. **7**, 785. doi : https://doi.org/10.3390/atmos15070785.